This article has been accepted for publication in a future issue of this journal, but has not been fully edited. Content may change prior to final publication. Citation information: DOI 10.1109/TMAG.2021.3053637, IEEE Transactions on Magnetics

Interaction of Tearing Modes with Passive Structures in a Tokamak

Paolo Bettini[1,2], Gianluca Spizzo[2], Dimitri Voltolina[2], Lionello Marrelli[2], Marc Maraschek[3], Valentin Igochine[3], Ruben Specogna[4], the ASDEX Upgrade Team[3] and the EUROfusion MST1 Team[*]

[1] Dipartimento di Ingegneria Industriale (DII), Università di Padova, Padova, Italy

[2] Consorzio RFX (CNR, ENEA, INFN, Università di Padova, Acciaierie Venete SpA), Padova, Italy

[3] Max-Planck Institute for Plasma Physics, Garching bei München, Germany

[4] Dipartimento Politecnico di Ingegneria ed Architettura (DPIA), Università di Udine, Udine, Italy

[*] see the author list of B. Labit et al., Nucl. Fusion **59** 086020

paolo.bettini@unipd.it

***Abstract*—In this work a surface current plasma model is coupled to a Volume Integral Formulation for studying the interaction between tokamak tearing modes and the machine metallic structures surrounding the plasma. By evaluating the passive response on a set of pick–up probes, tearing modes amplitude is estimated.**

***Index Terms*—Magnetic confinement fusion, eddy–currents, integral formulations, tearing modes.**

I. Physics Motivations

Among the major Magnetic Confinement Fusion (MCF) concepts under consideration, tokamaks are the most studied and have achieved the best overall performance in terms of triple product, the parameter that governs the extrapolation of present-day experiments to a real nuclear fusion reactor. Much of the phenomena happening in a typical tokamak discharge are due to *tearing modes* (TM), which are resonant perturbations of $\vec{B}$ directed across the flux surfaces: the name itself comes from magnetic surfaces which are broken and reconnected in the form of *magnetic islands*, influencing ion and electron transport which is greatly increased (or decreased, depending on particle collisionality) near the island [1]. Tearing modes are generally destabilized by a current density gradient in presence of finite plasma resistivity: if this current gradient is provided by the bootstrap current [2], the modes are given the name *neoclassical* TM, or NTM.

TM (or NTM) are directly or indirectly responsible for many pathological conditions in tokamak plasmas. For example, impurity accumulation and radiative instability inside a $m/n = 2/1$ island (with m, n the poloidal and toroidal mode numbers) is believed to cause the Greenwald density limit [3]; island overlapping gives birth to magnetic field stochastization and associated rapid electron energy loss [4]; last but not least, the abrupt termination of a tokamak discharge, i.e. what is referred to as a *major disruption*, is understood to be primarily due to the growth and braking of a single tearing mode, often the aforementioned $2/1$ NTM [5].

In the framework of the EUROfusion Medium Size Tokamak workprogramme, a high level topic is dedicated to disruption prediction and avoidance [6]: within this topic, a line of research consists in avoiding the disruption by stabilizing the $2/1$ (or $3/1$) TM through direct heating of the island with electron cyclotron current drive (ECCD) [7]. For an efficient heating of the island, an accurate identification of the resonant surfaces (from equilibrium reconstruction or electron cyclotron emission (ECE) measurements) and then of the position/width of the islands (from magnetics) is mandatory.

Previous work on ASDEX Upgrade (AUG) [8] aimed at describing the TM island in detail, by reconstructing the eigenfunctions of the main TM's during the disruptive phase of a high–density discharge [6]. The method simply consisted in a fit of cosine harmonics (amplitude and phase) extrapolated to the poloidal field ($\mathbf{B}_\theta$) pick–up probe measurements, using a well–known radial profile for the perturbed poloidal flux $\alpha_{m,n}(\psi_p)$ [9]. The method gave a reasonable topology of the internal magnetic field of AUG, with a $m/n = 2/1$ island of width ~ 6.3 cm, which is comparable with Electron Cyclotron Emission (ECE) measurements of electron temperature fluctuations in similar discharges. Nevertheless, passive structures surrounding the plasma, such as the Vacuum Vessel (VV) and the Passive Stabilization Loop (PSL), interact with the current produced by the TM, which possess frequencies in between 25 Hz and 10 kHz (1.7kHz in the case studied in [8]), and pollution in the $\mathbf{B}_\theta$ pick–up probe measurements has been already pointed out in the past [10]. The resulting topology (position and width) of the island could be substantially distorted by the systematic error in the probe measurements.

Purpose of this paper is to calculate and extract the systematic error in the pick–up probe measurements due to the eddy currents induced in the conducting structures surrounding the plasma by the rotating TM. To this end, an original model of the surface current associated to each resonant surface is adopted and it is coupled with a magneto quasi–static (MQS) integral formulation. As a result, the eddy currents induced by an arbitrary linear combination of rotating TMs can be computed (direct problem) and the real *structure* of each TM with periodicity m/n can be easily retrieved (inverse problem).

II. Modeling of Tearing Modes

We propose to introduce a model of surface current for TMs in which the current components are decoupled according to their periodicity (m/n); the following expression of the current density at each $n = 1$ mode resonance surface is then adopted:

$$\mathbf{J}_{m,n}(\mathbf{r}) = \nabla W(\mathbf{r}) \times \frac{\nabla \psi_p(\mathbf{r})}{|\nabla \psi_p(\mathbf{r})|}, \quad \mathbf{r} \in \Omega_p \qquad (1)$$

where ψ_p is the poloidal flux.

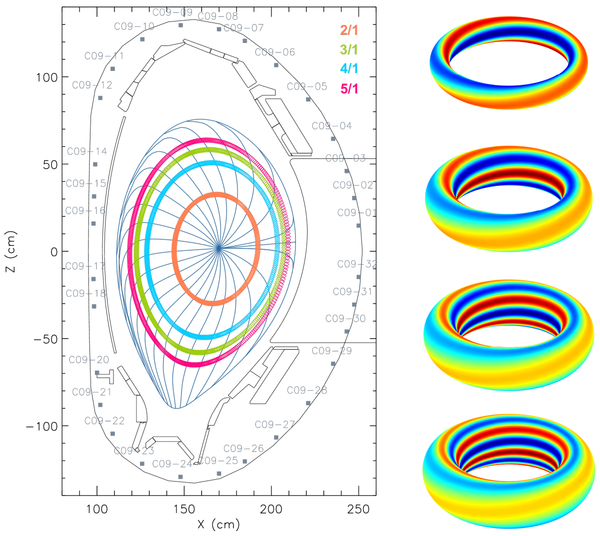

(a) (b)

Fig. 1: Resonance surfaces of periodicity m/n with $n = 1$ and $m = [2, \ldots, 5]$. (a) AUG radial section: mode 2/1 is the innermost (orange), 5/1 is the outermost (magenta). (b) Pattern of the scalar function $W(\mathbf{r})$ on each resonance surface. From top to bottom: 2/1, 3/1, 4/1, 5/1. A color scale is used to represent the value of W.

The scalar function W in (1) is expressed in terms of the TM eigenfunction of the harmonic with periodicity m/n as:

$$W(\mathbf{r}) = w_B[\cos(m\theta - n\phi) + i\sin(m\theta - n\phi)]\,\alpha_{m,n}\,e^{i\gamma_{m,n}}\,e^{i\omega t} \quad (2)$$

where $\alpha_{m,n}$ and $\gamma_{m,n}$ are the amplitude and the phase of the harmonic, ω is the angular frequency of rotation (known from experimental data, see section III-A), θ and ϕ are the poloidal and toroidal coordinates of the point $\mathbf{r} \in \Omega_p$.

The scalar function w_B in (2) depends only on the equilibrium configuration (flux density components (B_θ, B_ϕ), Jacobian of the flux coordinate system ($\mathcal{J}$), etc.) which can be obtained solving a consistent ideal MHD equilibrium constrained by the available diagnostic data:

$$w_B = \frac{mB_\phi + nB_\theta}{\mu_0 \mathcal{J} |\nabla \psi_p|} \quad (3)$$

Therefore, in the propose procedure, any TM is associated with two unknowns ($\alpha_{m,n}$, $\gamma_{m,n}$) which can be retrieved from the solution of an electromagnetic inverse problem with a suitable set of experimental measurements as input, as described in section III-B.

As an example, Figure ??-a) shows the projection of four resonance surfaces on a radial section of the device considered in section IV, AUG [8]. The pattern of the scalar function $W(\mathbf{r})$ on each resonance surface is shown in Figure ??-b).

III. Numerical approach

The structure of the code and the volume integral (VI) formulation used to solve the direct problem is presented in section III-A. The structure of the code used to solve the inverse problem is presented in section III-B.

A. Direct problem

The direct problem consists in calculating the entries (h, k) of the *transfer function* matrix $M(\omega)$ which links the k-th source (TM with periodicity m, n), rotating at a given angular frequency (ω), to the h-th synthetic measurement, including the effect of the eddy currents induced in the conducting structures surrounding the plasma, as shown in Figure 2. The code input are two current density distributions defined according to (1), in quadrature both in space and in time, with unitary amplitudes ($C_{m,n} = 1$, $S_{m,n} = 1$), to model the rotation of the k-th TM. The values of the quantities defined in (3), necessary to define the proper current density pattern (as those shown in Figure ??-b) come as output of an equilibrium code (e.g the CLISTE free boundary solver [11] can be used in AUG) and the angular frequency of rotation (ω) comes from a FFT of the experimental signals measured by a set of n_b magnetic sensors (pick-up coils).

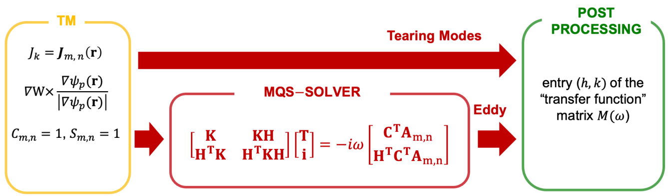

Fig. 2: Code structure for the solution of the direct problem.

The MQS-VI formulation proposed in this work relies on the Discrete Geometric Approach (DGA) and the use of the electric vector potential [13]. The electromagnetic (EM) fields are discretized on a pair of interlocked primal and dual grids of the conducting domain Ω_c surrounding the plasma region. The discrete Faraday's law enforced on dual faces in Ω_c is:

$$\mathbf{C}^T\mathbf{U} + j\omega\mathbf{C}^T\mathbf{A} = 0, \quad (4)$$

where $\mathbf{C}$ stores the incidences between primal faces and edges, $\mathbf{U}$ is the vector of the electromotive forces on dual edges and $\mathbf{A}$ stores the line integrals of the magnetic vector potential on dual edges.

We define the array of the currents across primal faces as

$$\mathbf{I} = \mathbf{C}(\mathbf{T} + \mathbf{H}\mathbf{i}), \quad (5)$$

where the arrays $\mathbf{T}$ stores the unknown line integrals of the electric vector potential on primal edges, while $\mathbf{i}$ is the independent currents vector of the first cohomology group generators of the domain boundary $\partial\Omega_c$, which incidences with the primal edges are expressed by $\mathbf{H}$.

Then the magnetic vector potential is separated in an unknown term due to eddy–currents and a known term $\mathbf{A}_{m,n}$ due to the current density $\mathbf{J}_{m,n}$ defined in (1).

Finally, the following discrete system is obtained:

$$\begin{bmatrix} \mathbf{K} & \mathbf{KH} \\ \mathbf{H}^T\mathbf{K} & \mathbf{H}^T\mathbf{KH} \end{bmatrix} \begin{bmatrix} \mathbf{T} \\ \mathbf{i} \end{bmatrix} = -i\omega \begin{bmatrix} \mathbf{C}^T\mathbf{A}_{m,n} \\ \mathbf{H}^T\mathbf{C}^T\mathbf{A}_{m,n} \end{bmatrix} \quad (6)$$

where $\mathbf{K} = \mathbf{C}^T(\mathbf{R} + j\omega\mathbf{M})\mathbf{C}$, with $\mathbf{R}$ and $\mathbf{M}$ being the resistance and magnetic matrices [13]. The effect of the conducting structures is evaluated at the pick-up probe positions, solving (6) for each prescribed m/n and ω values.

This article has been accepted for publication in a future issue of this journal, but has not been fully edited. Content may change prior to final publication. Citation information: DOI 10.1109/TMAG.2021.3053637, IEEE Transactions on Magnetics

The proposed formulation ends up with a dense system, a common drawback of integral methods. Nevertheless, the coupling of this formulation with a low-rank approximation technique based on hierarchical-matrix representation [14] allows to increase the size of the largest solvable problem on standard workstations, even far beyond the number of the Degrees of Freedom (DoFs) of the numerical model presented here (see for example [15]).

B. Inverse problem

The solution of the *inverse problem* is not addressed in the paper. However, for the sake of completeness, we summarise here the procedure for the case of n_{TM} Tearing Modes all rotating at the same angular frequency (ω).

The n_{TM} couples of unknowns ($\alpha_{m,n}$, $\gamma_{m,n}$) can be retrieved as follow (see Fig. 3):

1) Assembling of the LHS: complex matrix of dimension $n_b \times n_{TM}$; each entry $M_{h,k}(\omega)$ comes from the solution of the direct problem
2) Assembling of the RHS: complex array of dimension $n_b \times 1$; each entry $\bar{B}_k = B_k\, e^{i\beta_k}$ comes form the FFT of pick-up probes signals
3) Solution of the overdetermined complex linear system of dimension $n_b \times n_{TM}$ (Moore-Penrose pseudoinverse)

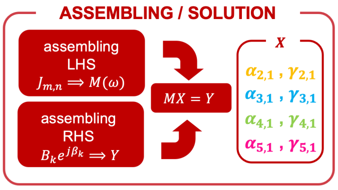

Fig. 3: Assembling the complex linear system of dimension $n_b \times n_{TM}$ and solving for the n_{TM} couples of unknowns.

IV. Numerical Results

In this paper, the proposed procedure is applied to the AUG device [8]. The two main conducting structures surrounding the plasma are here considered:

- the Vacuum Vessel (VV), a complex stainless steel structure with several apertures (ports) for diagnostics, heating, and vacuum systems (Figure 4-a).
- the Passive Stabilisation Loop (PSL), a massive copper conductor for passive plasma stabilisation (Figure 4-b).

To asses the effect of the conducting structures, three different direct problems have been solved, modelling only the VV or the PSL or both, respectively. The number of elements of the primal complex (nodes, edges, faces, volumes) and DoFs for the three cases are shown in Table I.

In the experimental campaigns in AUG, a number of TMs with comparable amplitudes can be observed, often rotating at the same frequency. For the sake of simplicity, here we consider two modes with periodicity $m/n = 2/1$ ($\alpha_{2,1} = 1$, $\gamma_{2,1} = 0$) and $m/n = 3/1$ ($\alpha_{3,1} = 1$, $\gamma_{3,1} = 0$), rotating at $1.7\,kHz$, as the source terms of the direct problem. Figure 5 shows the patterns of the flux density produced by these

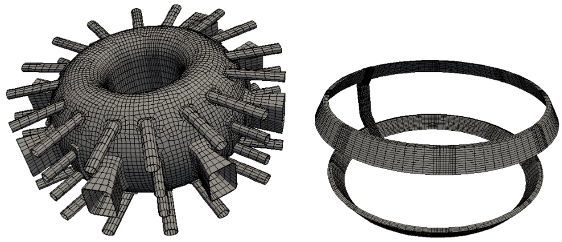

(a) (b)

Fig. 4: Main conducting structures surrounding the plasma in the AUG device [8]. (a) VV: discretised with 16287 hexahedra. (b) PSL: discretised with 17664 hexahedra.

		VV	PSL	VV+PSL
nodes	N_n	31945	24938	56883
edges	N_e	79940	67159	147099
faces	N_f	64226	59884	124110
volumes	N_v	16287	17664	33951
DoFs	N	17210	28437	45647

TABLE I: Number of elements of the primal complex and DoFs for the three cases studied (VV, PSL, both).

modes in the actual positions of pick-up coils ($C09 - xx$) at an arbitrary time instant t_0: it is worth noting that they are almost in phase in the low field side ($\theta \approx 0$) and out of phase in the high field side ($\theta \approx \pi$).

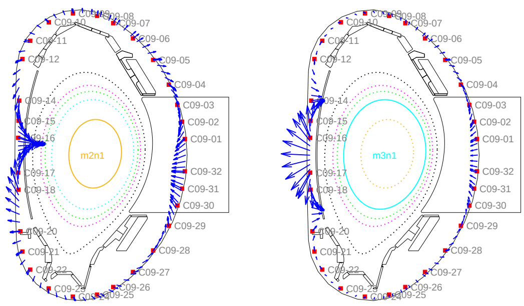

(a) (b)

Fig. 5: Single TMs rotating at $1.7\,kHz$: flux density produced at an arbitrary time instant t_0. (a) $m/n = 2/1$. (b) $m/n = 3/1$.

It is interesting to observe the reaction fields (effect of the eddy currents induced in the conducting structures) when only the VV or the PSL are modelled. As expected, the effect of the PSL is mainly concentrated in the region behind it, while the effect of the VV is more pervasive and it is particularly noticeable in the high field side where the source term is larger, as shown in Figure 6. Moreover, the effect of the VV tends to reinforce the actual field at the magnetic sensors positions w.r.t. the ideal case (field produced only by TMs) as shown in Figure 7, while the effect of the PSL tends to reduce the actual field behind it (e.g. by sensors $C09 - k$ with $k = [2, 3, 4, 29, 30, 31]$), as shown in Figure 8. Figures 7–8 refer to the $m/n = 2/1$ case. Similar considerations apply also to the $m/n = 3/1$.

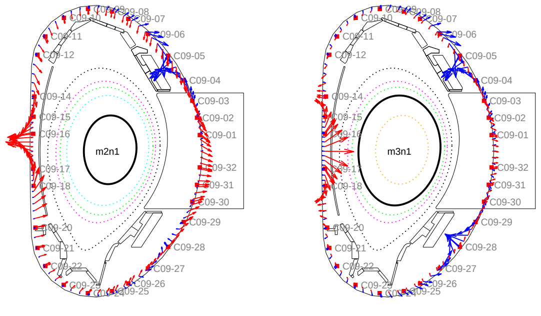

(a) (b)

Fig. 6: Flux density generated by the eddy currents induced in the VV (red) and in the PSL (blue) at t_0 for a single TM rotating at $1.7\,kHz$: (a) $m/n = 2/1$; (b) $m/n = 3/1$.

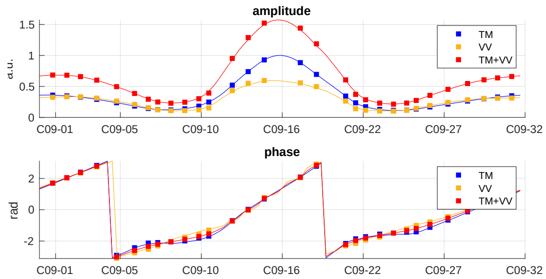

Fig. 7: $m/n = 2/1$: VV effect on amplitude and phase of the actual signals (pick-up coils $C09 - xx$) w.r.t. the ideal case.

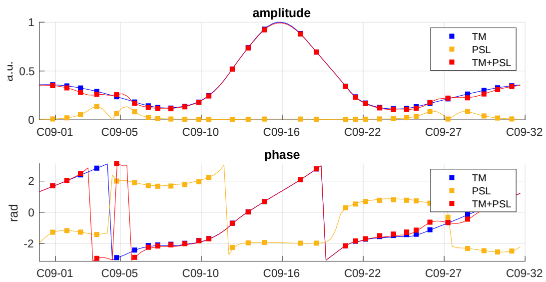

Fig. 8: $m/n = 2/1$: PSL effect on amplitude and phase of the actual signals (pick-up coils $C09 - xx$) w.r.t. the ideal case.

Finally, we consider a linear combination of two modes with periodicity $m/n = 2/1$ ($\alpha_{2,1} = 1$, $\gamma_{2,1} = 0$) and $m/n = 3/1$ ($\alpha_{3,1} = 1$, $\gamma_{3,1} = 0$), rotating at $1.7\,kHz$, to evaluate the global effect of VV and PSL. Figure 9 shows a comparison in terms of amplitude and phase of the synthetic measurements for the single modes, their linear combination and the actual signals which take into account the effects of VV and PSL. It is worth noting that should the effect of VV and PSL be neglected, the current densities at the resonance surfaces would be significantly different w.r.t. the *real* ones and the resulting topology (position and width) of the island substantially distorted.

V. Conclusion

The proposed approach provides a simple procedure, requiring an equilibrium reconstruction and a MQS solver, to get the correct value for the TM current density at the

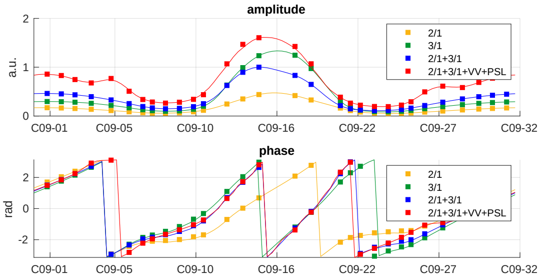

Fig. 9: Comparison of the actual signals (red) at pick-up coils ($C09 - xx$) w.r.t. the ideal case (blue) for a linear combination of two modes with periodicity $m/n = 2/1$ and $m/n = 3/1$.

resonance surface which can be used for physics studies (e.g. coupled to a guiding center code), or integrated in real-time algorithms for disruption prediction and control.

VI. Acknowledgements

This work has been carried out within the framework of the EUROfusion Consortium and has received funding from the Euratom research and training programme 2014-2018 and 2019-2020 under grant agreement No 633053.

References

[1] R.B. White, *The Theory of Toroidally Confined Plasmas,* 2nd ed., Chapter 5, pp. 151–166, Imperial College Press, London, 2001.

[2] R.B. White, et al, "Saturation of the tearing mode," *Physics of Fluids (1958-1988),* vol. 20, no. 5, pp. 800–805, May.1977.

[3] D.A. Gates and L. Delgado-Aparicio, "Origin of Tokamak Density Limit Scalings," *Phys. Rev. Lett.,* vol. 108, no. 16, 165004 (4pp), Apr.2012.

[4] A.B. Rechester and M.N. Rosenbluth, "Electron Heat Transport in a Tokamak with Destroyed Magnetic Surfaces," *Phys. Rev. Lett.,* vol. 40, no. 1, pp. 38–41, Jan.1978.

[5] H. Zohm, *MHD Stability of Tokamaks,* pp.191–199, Wiley-VCH, 2015.

[6] M. Maraschek *et al.* , "Path-oriented early reaction to approaching disruptions in ASDEX Upgrade and TCV in view of the future needs for ITER and DEMO," *Plasma Phys. Control. Fusion,* vol. 60, no. 1, 014047, Jan.2018.

[7] B. Esposito, G. Granucci *et al.*, "Disruption control on FTU and ASDEX upgrade with ECRH," *Nucl. Fusion,* vol. 49, no. 6, 065014, Jun.2009.

[8] G. Spizzo, R.B. White, M. Maraschek, V. Igochine, G. Granucci, and the AUG Team, "Nonlocal transport in toroidal plasma devices," *Nucl. Fusion,* vol. 59, no. 1, 016019 (14pp), Jan.2019.

[9] J. P. Meskat, H. Zohm, et al., "Analysis of the structure of neoclassical tearing modes in ASDEX Upgrade," *Plasma Phys. Control. Fusion,* vol. 43, no. 10, pp. 1325-1332, Oct.2001.

[10] M. Schittenhelm and H. Zohm, "Analysis of coupled MHD modes with Mirnov probes in ASDEX Upgrade," *Nucl. Fusion,* vol. 37, no. 9, p. 1255, Sep.1997.

[11] Schneider, W., et al, "ASDEX Upgrade MHD equilibria reconstruction on distributed workstations," *FED,* 48 (1), pp. 127-134

[12] R. Albanese and G. Rubinacci, "Integral formulation for 3D eddy-current computation using edge elements," *IEE Proceedings A - Physical Science, Measurement and Instrumentation, Management and Education - Reviews* 135 (7), pp. 457-462, 1988

[13] P. Bettini, M. Passarotto, and R. Specogna, "A Volume Integral Formulation for Solving Eddy Current Problems on Polyhedral Meshes," *IEEE Trans. Magn.,* vol. 53, no. 6, Jun.2017.

[14] R. Kriemann, "HLIBpro (v2.6)," *http://hlibpro.com*, Accessed: 2017-11-01

[15] D. Voltolina, P. Bettini, P. Alotto, F. Moro, R. Torchio, "High-Performance PEEC Analysis of Electromagnetic Scatterers," *IEEE Transactions on Magnetics*, 55 (6), art. no. 8638854